

Fatigue Crack Propagation at the Bone/Cement Interface

John W. Steege Northwestern University Rehabilitation Engineering Program
MSME Chicago, Illinois, 60611

Jack L. Lewis University of Minnesota
PhD Department of Orthopaedic Surgery
 Mayo Memorial Building
 420 Delaware St.
 SE Box 289
 Minneapolis, Minnesota, 55455

Richard L. Wixson Northwestern University Medical School
MD Department of Orthopaedic Surgery
 303 E. Chicago Ave.
 Room 9-002
 Chicago, Illinois, 60611

Terry Nicola Director of Sports Medicine
MD,MS Spaulding Rehabilitation Hospital
 125 Nashua St.
 Boston, Massachusetts, 02114

Send proof and reprint requests to :

John W. Steege
Northwestern University Rehabilitation Engineering Program
345 E. Superior
Room 1441
Chicago, Illinois 60611

(312) 908-6531

Running Title: Bone/Cement Interface Fatigue

Copyright 1988, 1995 by John W. Steege

ABSTRACT

A method for creating and measuring crack propagation under tensile cyclic loading at a bone/cement interface has been developed and used to measure the rate of crack propagation as a function of stress intensity factor, cement penetration depth, and bone strength. Results from 26 specimens show the cracks to propagate, but interrupted periodically by what is suspected to be cement posts. For the propagation region, propagation is approximately proportional to the square of the stress intensity factor, inverse to the cube of the penetration depth, and inverse to the square of the bone strength. Although statistically significant to the .05 level, the fitting relationship accounts for only approximately 60% of the variance.

Based on the observation that cement posts appear to be responsible for retarding crack growth, artificial posts, both cement and metal, are proposed as a method to improve fixation. Three specimens were tested with a prototype post-type crack arrestor. These showed fatigue strengths as great or greater than any of the test specimens, suggesting this method has merit as a means of enhancing implant fixation.

Keywords: Bone-Cement; TJR Interface; Bone/Cement Interface Strength

INTRODUCTION

Loosening of prosthetic joint components secured to bone with PMMA (polymethyl-methacrylate) bone-cement remains a concern with these devices. There are current attempts to perfect bony ingrowth fixation techniques, but it is likely that even with its shortcomings, cement fixation will have significant applications for the foreseeable future.

Fixation of joint replacement components to bone by polymethylmethacrylate bone-cement is achieved by a mechanical interlock of the cement into porous, trabecular cancellous bone. The first mechanical tests performed on the interface were simple tensile and shear tests [1,12,13,26]. These experiments generally found that mechanical strength did indeed increase with increasing penetration and pressurization to insert the cement. Some of these researchers, noting that increased usage of PMMA had been shown to lead to increased bone necrosis, increased levels of monomer in the blood stream, and increased PMMA debris in the joint, suggested optimal cement penetration depths based on these tensile and shear tests. These recommended values range from 3 to 4 mm [1,26].

Loosening of total joint components fixed with bone-cement is a problem that continues to arise. It has been postulated that the appearance of a radiolucent line at the bone/cement interface in radiographs of total joint implants is an indication of loosening [20]. Radiolucencies around total joint replacements are commonplace with all follow-up studies of hip and knee replacements reporting them to at least a small degree. Often, a thin fibrous tissue is found at the bone-cement interface, and is thought to be the radiolucency on x-ray [5,9,19,25]. This tissue has been associated with and

has been considered a precursor to component idiopathic loosening. Debate continues as to why this fibrous liner forms. Some investigators have proposed that its formation is the result of a biological reaction to load environment and/or implant material [9,19]. Alternatively, it has been suggested that the tissue growth follows mechanical failure of the interface [5]. This mechanical failure could be viewed as crack growth through the bone, the cement, the bone/cement interface, or any combination of these. It is this second postulate, that component loosening is due to mechanical failure of the bone/cement interface, that is related to the work in this paper.

Several researchers have examined the fracture properties of bone. Most of the studies have involved push-out tests on bovine bone. Fracture mechanics measurements on both three-point bending and compact tension specimen tests have been performed on compact bone. Mean critical stress intensity factors (K_{IC}) of 3.5 to 4.0 MPam^{1/2} have been reported respectively [3,27]. Few studies have been performed on human cancellous bone due mostly to limitations on specimen size.

Failure and breakage of the cement has been documented *in vivo* [25]. Crack growth was proposed early as a mechanism for cement failure [2,10,23]. Subsequently, much work was done comparing the critical stress intensity factors and energy release rates for various clinical cements, experimental cements, and cement preparation and application techniques [21,22,24]. Others have made similar comparisons using cement fatigue strength or fatigue life as their criteria [11,24]. The load rates used by these investigators ranged from 2 to 23 Hz while fatigue testing cements in fully reversed tension-compression cycles. O'Conner et al. [18], however, found a significant increase in cement fatigue life when tested at 2 Hz as compared to 20 Hz.

The most likely region of fracture failure is at the interface itself. Some work has been done in this area and is the topic of this paper. Mak [16] tested compact tension specimens composed of fixed bone and Simplex-P bone-cement and found rough relationships between PMMA interdigitation and the critical stress intensity factor. He concluded that if a tensile stress of 1 MPa is present at the edge of a tibial component (a stress predicted by Askew, et al.[14]), flaws as small as 1-2 mm could initiate cracks in poor (low cement penetration) interfaces. Flaws of this size can commonly be seen in clinical radiographs. Mak's study used single cycle tests and generally involved low cement penetration values.

Nicola [17] performed four-point bending fracture fatigue tests and used a finite element analysis [6] of his specimen configuration to determine the applied cyclic stress intensity factor. He frequently noted formation of a secondary crack through cement spicules after a primary crack had propagated through the entire bone/cement interface. Propagation of this second crack would lead to catastrophic failure. Other phenomena of note were formation of a crack in compression regions, micromotion between cement and bone ahead of the crack tip, and fluid flow between cement and bone. A

rough relationship was found between the cyclic stress intensity factor and the crack propagation rate. Lewis et al. [15] concluded that possibly no cement/bone interface would be completely resistant to fatigue.

Clech et al. developed mathematical models for the tension and compressive crack situation [7]. Both models employ a cohesive zone along a portion of the propagating crack. They modeled the cohesive zone as a set of linear springs whose stiffness was obtained experimentally. They used a comparative finite element analysis similar to [6] for the four-point bending test configuration pictured in Figure 1 in order to determine the stress intensity factor in relation to crack length for interfaces modeled with and without a cohesive zone. It was found that inclusion of a cohesive zone slightly reduced the stress intensity factor at the crack tip and that the magnitude of this reduction increased with increasing cohesive zone length.

The work described in the remainder of this paper builds on this previous work, extending the experimental work of Nicola. Bone/cement specimens suitable for use in a four-point bending specimen are fabricated and tested in cyclic loading in a hydraulic materials test machine (Model 810, MTS Inc., Minneapolis, MN). Crack propagation length is monitored versus cycle number. Stress intensity is determined using the finite element method of Clech et al., and data reduced to crack propagation rate as a function of stress intensity factor, cement penetration depth, and bone strength. The rationale for testing the bone strength was that the strength is related to the porosity [4], which would be expected to be related to the ability to penetrate the cement into the bone, while also representing some portion of the interface. Based on the resulting data, prototype devices are made and used to reduce interface susceptibility to crack propagation.

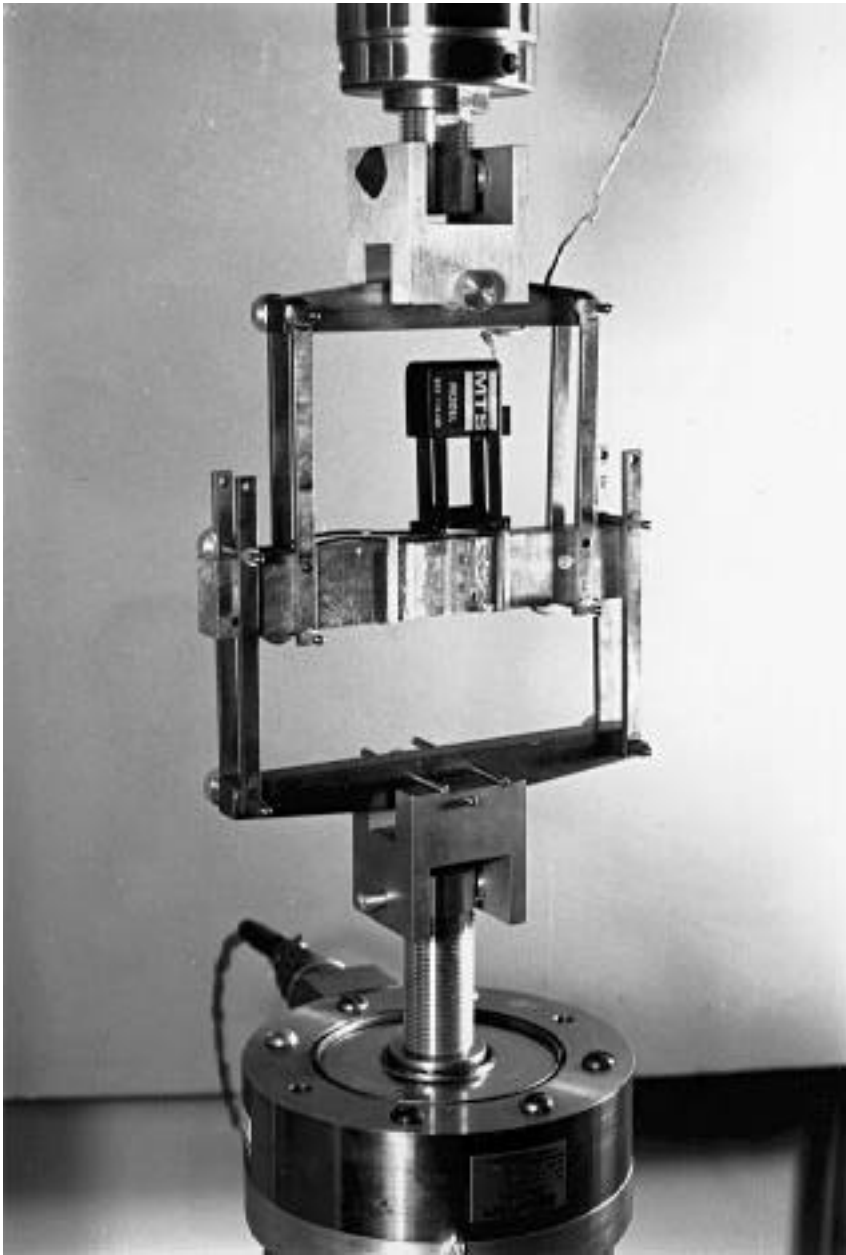


Figure 1: Photograph of the final four-point bent beam test configuration. Note the clip gage attachment (MTS) across the crack mouth.

METHODS

Nomenclature

a_p	: primary crack length (mm)	P_{sig}	: statistical significance based on F value
a_s	: secondary crack length (mm)	PEN	: penetration of cement in millimeters
BSG	: grade of the bone strength (1, 2, 3) as defined	Post _N	: # of discontinuities (posts) along an interface
Δa	: crack extension in millimeters	r	: multiple correlation coefficient
$\Delta a/\Delta N$: crack propagation rate in millimeters per cycle (variance in dependent variable)	r^2	: square of r
ΔK	: cyclic stress intensity factor in MPam ^{1/2}		explained by the independent variables in
ΔN_{post}	: number of cycles to pass through a given post		a linear relationship)
∂	: cohesive zone length in mm ($a_p - a_s$)		

Experimental

Fresh cancellous bone was taken from several distal femora and proximal tibiae obtained from amputation or autopsy and which had been stored frozen at -22° Celsius. Bone was cut into rectangular specimens 25 x 15 x 12.5 mm in dimension on a low speed rotary thin sectioning saw. All bone specimens were taken from within 1 cm from the joint's articulating surface. The 12.5 mm dimension was oriented parallel to the long axis of the donor bone. From the remaining bone most proximal to the joint, 5 x 5 x 5 mm bone cubes were cut (for compressive bone strength tests described later) which corresponded to the 25 x 15 mm surface of the rectangular bone specimens. All bone was then stored frozen at -22° Celsius until it was fashioned into four-point bending specimens or compressively tested.

The exact cross-sectional area of the 5 x 5 x 5 mm bone blocks was measured with a micrometer. The cubes were compressively loaded to yield in the direction of the long axis of the donor bone at a displacement rate of 0.4 mm/min on the MTS. The compressive strength of each cube was calculated from the yield load and the measured cross-sectional area of each cube. An average compressive strength of the 12 cubes which corresponded to the interfacial region was determined for each specimen. Bone strength values were also classified into three grades where: 1 was < 3 MPa, 3 was > 6 MPa, and 2 was in between.

To form the four-point bending specimens, the large bone cubes were placed at the bottom of a jig such that the 25 x 15 mm surface which had been proximal to the articulating knee joint was face up and clamped into place. To pre-form

an initial 5 mm crack, a 100 μm thick razor blade was placed into a groove of the jig so as to be wedged over approximately 15 x 5 mm of bone surface .

Simplex-P Bone-Cement was poured into the jig until it completely covered the top of the bone surface at a thickness of approximately 10 mm. A piston was then slipped into the jig and lowered until it rested on top of the cement. The assembly was placed on the ram of the MTS. At 135 seconds from the beginning of the cement mix, the piston was loaded for five seconds to create application pressures as reported in Table I. The assembly was removed from the ram and the cement allowed to set. Using a second jig, aluminum bars each weighing 70 grams were fastened to both ends of the specimen using PMMA. After formation of the interface, the test piece, now in the form of a beam, was placed into a refrigerator at 5° Celsius to await testing the following day.

Zero magnification x-rays of the specimen were taken to determine depth of penetration of the cement into the bone. The approximately 20 mm interface was divided into four equal zones. Using a micrometer, the maximum depth of penetration for each zone was determined and the mean for the entire interface calculated. The radiographs of the specimens were also examined by three independent observers and their degree of penetration graded on a scale of one to three, with one being low and three being high. Good agreement was found between the measured values and the observer grades.

For testing, the beam specimen was warmed to room temperature and to assist in visual monitoring of crack growth, a small scale attached onto the PMMA adjacent to the approximately 20 mm long visible interface. A one inch gage length extensometer was affixed across the initial crack mouth by use of elastic bands and was used to measure crack mouth opening. This assembly was placed in a four-point bending jig which was suspended between the load cell and ram of the MTS (Figure 1). Thus load was measured either as a function of ram stroke or crack mouth opening on an X-Y plotter. Load was applied linearly from no load to full bending and then linearly relieved. Specimens were loaded at between 1.0 and 1.67 Hz.

Primary and secondary crack growth was measured visually through a triocular microscope. Measurements were usually made at 13x magnification and were facilitated by a 100 division vernier in one of the eyepieces and the attached scale. At each recording of crack length (recorded on a regular basis), the number of cycles was documented and the X-Y plotter was activated yielding a load vs crack mouth opening curve. The triocular scope allowed for photographic, motion picture, and video documentation of specimens.

Definition of the crack tip was difficult but was accomplished by adhering to the following criteria. For the primary crack, the tip was defined as the point on the interface where motion between the bone-cement and bone originated and was continuous back to the initial crack tip. The tip of the secondary crack was defined as the point where separation

between the cement and bone edges was approximately 130 μm . This width was selected after observation of various specimens.

Specimens were loaded each working day to maximum loads ranging from 35 to 489 Newtons. If the pre-formed initial crack was ignored and simple beam theory employed, these loads would create approximate maximum tensile stresses of between 0.2 to 3 MPa, which are in the range of values predicted by some finite element analyses of total joint implants. Cyclic loading continued in this fashion until approximately 500,000 cycles had been reached or until catastrophic failure of the interface. The specimens were kept soaked by saline drip during all testing. In all, 26 specimens were prepared and tested. Of all the specimens, 8 were of tibial stock while 18 were of femoral stock. Data for all test specimens is presented in Table I.

Data Analysis

In accordance with the results of Nicola [17], two cracks were seen at the interface (Figure 2). The first crack, henceforth referred to as the primary crack (a_p), was the leading crack and would form between the bone and cement. The other crack, henceforth referred to as the secondary crack (a_s), would follow the primary crack and grow through a combination of cement, bone, and interface. This secondary crack can be thought of as the end of the cohesive zone modeled by Clech [7]. A typical interface with both crack types is pictured in Figure 3. Due to the dynamic nature of the primary crack, only the secondary crack may readily be seen on still photographs. Motion picture and video documentation of the cracks exists for demonstration purposes.

The data resulting from these procedures were crack length as a function of cycle number and load, with corresponding cement penetration depth (PEN) and bone strength (BSG) for each specimen. The cyclic stress intensity factor (ΔK) was determined for both a_p and a_s using the results of Clech [6]. Its value was determined for each crack length with and without the effects of a cohesive zone.

Data was analyzed by multiple regression, assuming various forms of functional relationships between dependent and independent variables. For each multiple regression analysis subsequently reported, variable transformations were performed to allow for linear-linear, linear-log, log-linear, and log-log analyses. Without exception, the log-log (power law) regressions provided the most highly correlated results. Similarly, analyses was performed with both ordinal and categorical values of penetration and bone strength with best results being obtained for ordinal values of penetration (PEN) and categorical values of bone strength (BSG). For clarity, these are the only statistical results reported.

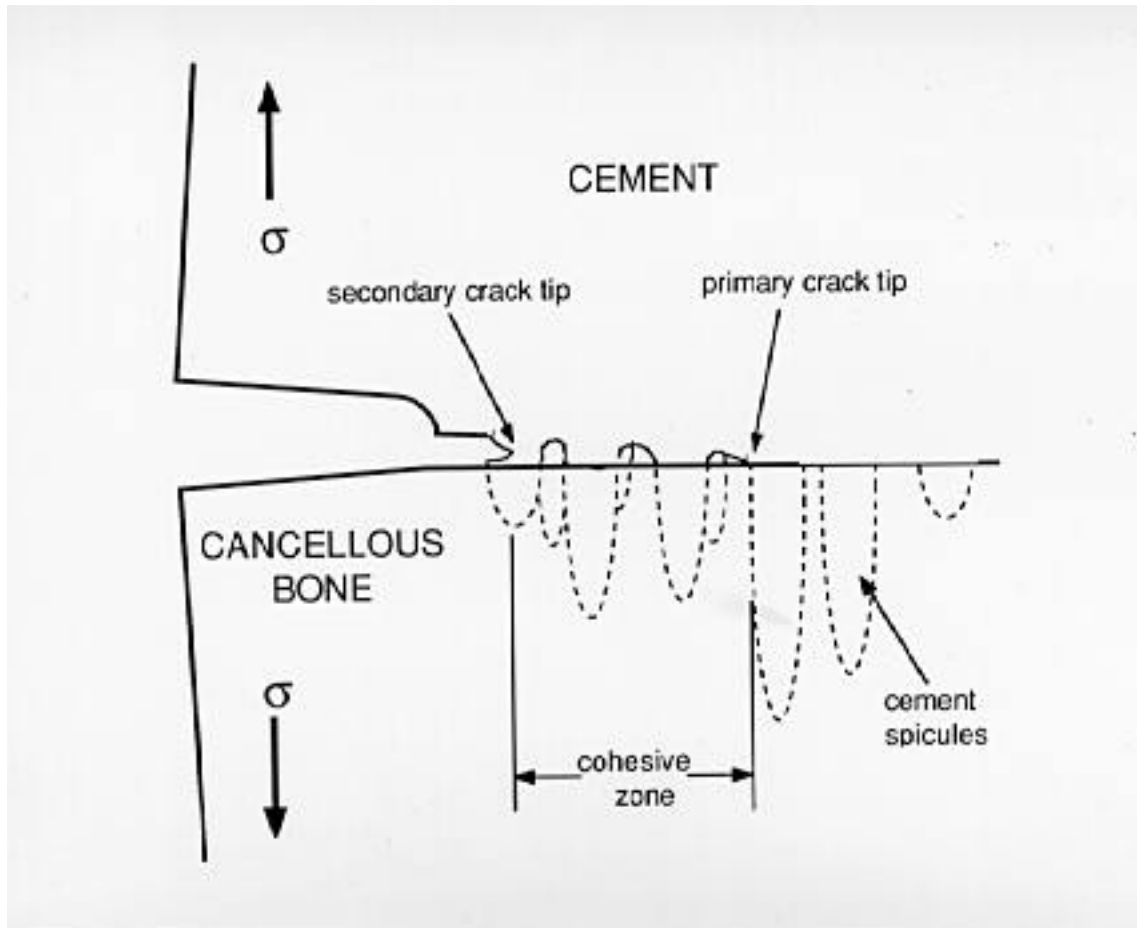


Figure 2: Schematic of the primary crack and cohesive zone as modeled by Clech.

Attention was directed at the primary crack with the assumption that the secondary crack simply defines a cohesive zone (δ) which forms behind the primary crack. Plots of primary crack length versus cycle were generated for each specimen and typically were of the form of Figure 4.

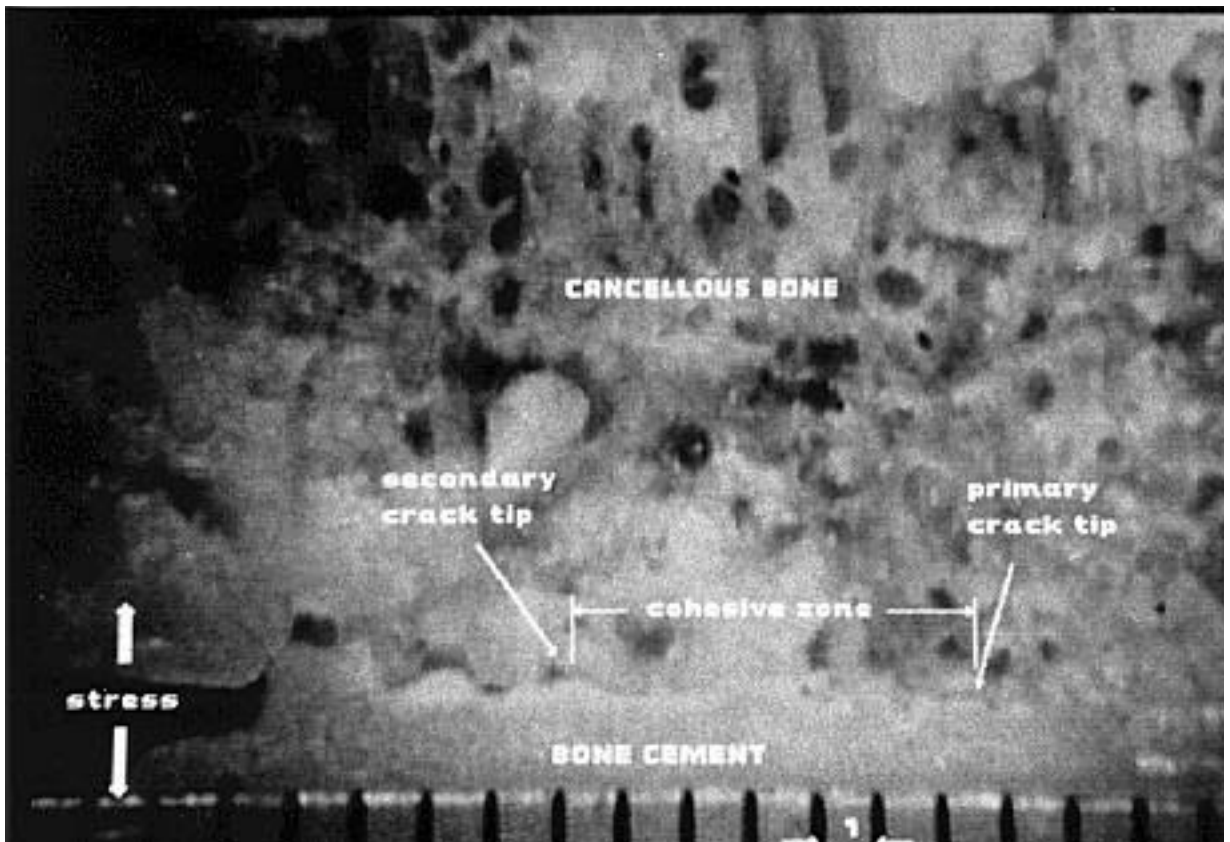


Figure 3: Specimen S10a in bending under 67 Newtons of load after 533,000 cycles at 178 Newtons of load. The initial preformed crack is on the left.

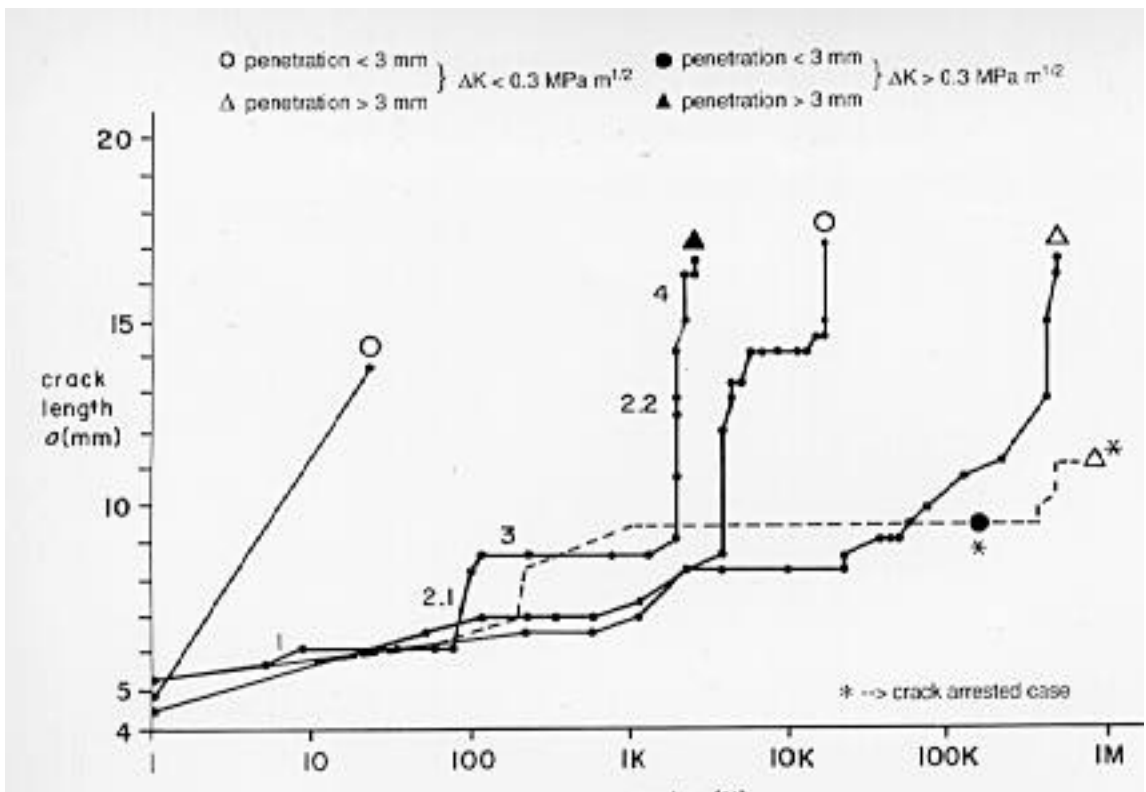


Figure 4: Plot of primary crack length vs $\ln\{\text{cycle}\}$ as a function of cement penetration depth and stress environment for several specimens used in the study. Note the specimens marked with a * correspond to the posted specimens A5d (Δ) and A6d (\bullet).

General patterns of crack propagation were observed, suggesting the definition of different regions of propagation. The behavior of a_p in the four-point bending tests was divided into four regions as depicted in one of the specimens of Figure 4. These regions were then defined as follows:

4. These regions were then defined as follows:

1. The primary crack has just begun and it is free of any cohesive forces. This is a relatively short lived effect where the crack extension (Δa) is small, the cohesive zone length ($\bar{\sigma}$) is small or nonexistent, and the number of cycles (ΔN) is low.
- 2.1 As the crack length extends past region 1, the cohesive zone forms. The presence of cohesive forces in this zone reduces the stress applied at the crack tip from what it would be without a cohesive zone as demonstrated by Clech [8]. In general, this region of growth is quite linear and constant.
3. There appear discontinuities in the propagation of the crack which are defined as region 3. These are hypothesized as occurring due to the crack tip encountering a large PMMA post(s). The crack then requires a given number of cycles, ΔN_{post} , to propagate through or around the post. The magnitude of ΔN_{post} will depend upon the mean post size and its stress environment. The mean post size can be considered a function of cement penetration level and the specimen's bone density or strength.

Also, multiple instances of these discontinuous regions may occur in each specimen. The number of discontinuities along an interface (Post_N) may possibly be described by crack length, cement penetration level, and bone strength.
- 2.2 Crack propagation is occurring via the same mode as in 2.1 after a discontinuity has been overcome. Similarly, as mentioned above, additional discontinuities may be encountered.
4. Failure through the cohesive zone has and is occurring, and in a good number of cases is continuing through the bone. This region is primarily the result of quick and catastrophic propagation of the secondary crack.

By breaking the behavior of the crack into the regions described, it was thought that descriptive equations for each region could more completely describe the propagation of the primary crack. Using linear regression analysis, values of $\Delta a/\Delta N$ were calculated for each region of every specimen. Except for region 4, the linear correlation coefficients were high ($r > 0.9$). The $\Delta a/\Delta N$ values (or slope of the linear regression equation) were then compiled into separate data files of each region along with associated bone strength, penetration, crack length, and stress intensity values. The occurrences of discontinuities (region 3) were also identified from plots of the crack propagation data and their duration.

in cycles, bone strength, penetration, crack length, and stress intensity values associated with each occurrence were recorded and stored in a separate data file. Multiple regression analyses were performed on each data file to provide descriptive equations of crack growth in each generalized region as a function of its descriptor variables.

RESULTS

The typical crack mouth opening was of the order of 120 μm as measured by the extensometer during stable crack growth and the maximum measured, just preceding catastrophic failure, was 800 μm . Table I presents initial crack opening data. To determine the amount of initial crack opening measured by the extensometer due to interface separation as opposed to material deformation, a 3-D finite element model (8 noded linear isoparametric brick elements) of the beam specimen was created and analyzed using SAP IVTM. A crack length of 5 mm, cancellous bone modulus of 0.33 GPa, and PMMA modulus of 2.1 GPa were given to the model. A load of 178 Newtons was applied to the model to simulate the experimental four-point bending situation. Nodes were identified on the model which corresponded to the attachment points of the extensometer. The finite element analysis calculated displacement between these points in the crack opening direction was 55 μm . For the actual specimens which were loaded to 178 Newtons (mean bone strength 5.8 MPa; mean initial crack length 4.9 mm) the resulting mean initial crack mouth opening was 49 μm . By using linear regression, the crack mouth opening as measured by the extensometer was found to significantly increase with a_p ($r^2 = 0.50$).

Permanent deformation of the interface after cyclic loading was also noted. This phenomenon was further demonstrated by observing the output of the extensometer attached across the crack mouth. After each cycle, the zero point of the gage would linearly increase by a small amount, indicating that the cement and the bone had separated slightly. Optical measurement of the attachment points of the gage assured that the extensometer was not slipping relative to the interface.

Region 1 was studied, but in general the number of cycles in region 1 was small. Likewise the number of cycles in region 4 was small while the propagation rate was nonlinear and the propagation mode irregular. Therefore, regression results for region 4 are not reported.

When all data except that in regions 1 and 4 were lumped together (considering crack propagation through regions 2 and 3 to be continuous) the resulting regression equation was:

$$\Delta a / \Delta N = (2.5 \times \Delta K^{2.4}) / (\text{PEN}^{2.9} \times \text{BSG}^{3.1}) \quad r^2 = 0.59 \quad \{1\}$$

The coefficient in this equation was not statistically significant.

Analysis was performed considering the effects of modeling the discrete regions 2 and 3. The total number of cycles was generalized as:

$$\Delta N_{\text{total}} = \Delta N_2 + \Sigma[\Delta N_3] \quad \{2\}$$

ΔN_2 is the expression for region 2 and represents regions 2. {1,2,... n} along an interface. It expresses the number of cycles an interface is in steady propagation as a function of the cyclic stress intensity at its crack tip, the bone strength, the depth of cement penetration, and the crack length.

$\Sigma[\Delta N_3]$ represents the number of discontinuities or posts along an interface multiplied by the number of cycles needed to pass through each post. It is expressed as:

$$\Sigma[\Delta N_3] = \text{Post}_N \times \Delta N_{\text{post}} \quad \{3\}$$

Post_N can be expressed as a function of the crack length, the bone strength, and the depth of cement penetration.

Similarly, ΔN_{post} can be expressed as a function of the cyclic stress intensity at the crack tip, the bone strength, and the depth of cement penetration.

Combining equations {2} and {3} yields:

$$\Delta N_{\text{total}} = \Delta N_2 \{ \Delta K, \text{BSG}, \text{PEN}, \Delta a \} + [\text{Post}_N \{ \Delta a, \text{BSG}, \text{PEN} \} \times \Delta N_{\text{post}} \{ \Delta K, \text{BSG}, \text{PEN} \}] \quad \{4\}$$

ΔN_2 , Post_N , and ΔN_{post} were all obtained in terms of their independent variables by multiple regression analysis for all the specimens. Placing these into {4} yielded (in mm/cycles):

$$\frac{\Delta a}{\Delta N_{\text{total}}} = \frac{\Delta K}{\text{PEN}}^{2.2} \times \frac{1.3}{\text{BSG}^{2.3} + 9.4} \times \frac{\Delta K^{0.20}}{\text{PEN}^{1.2} \times \text{BSG}^{3.0}} \quad \{5\}$$

which describes crack growth for regions 2 and 3. All of the exponents and coefficients of this equation are significant to the 0.05 level. This equation is shown for two different interface types in Figure 5.

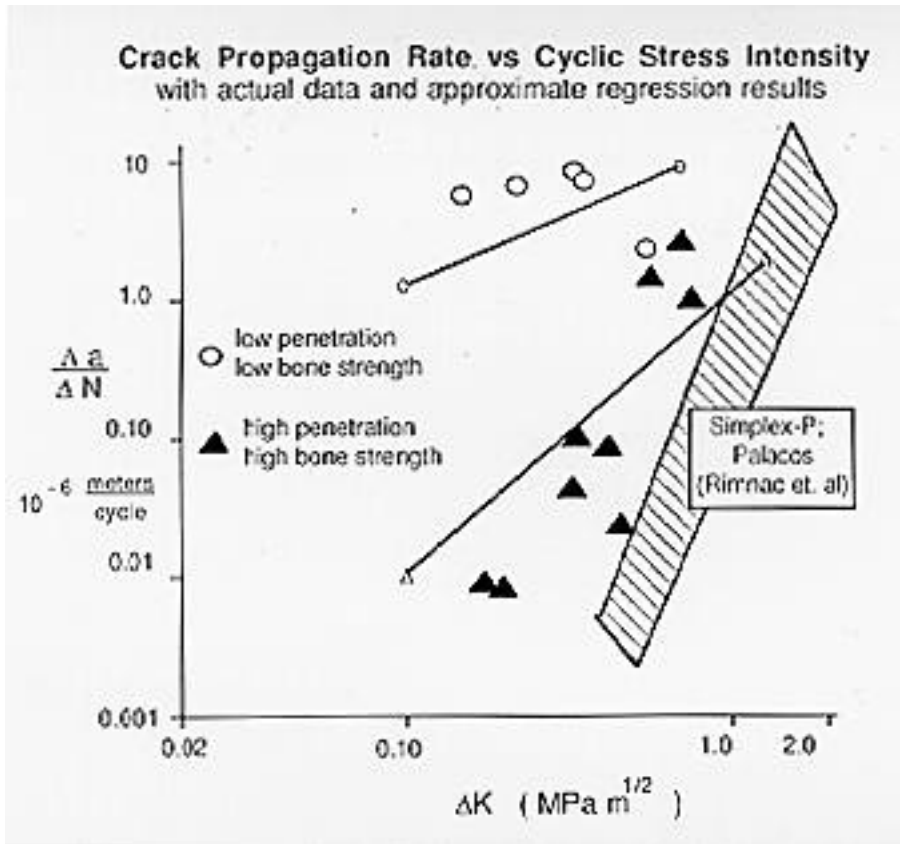


Figure 5: Crack propagation rate vs cyclic stress intensity factor with selected actual data and corresponding predicted results from equation {5}.

To determine the accuracy of the predictive equation {5} in forecasting crack growth with respect to actual data, a descriptive parameter similar to multiple r^2 was developed. The parameter, which will simply be equated with r^2 , was of the form:

$$r^2 = 1 - \frac{\sum (x_i - c_i)^2}{\sum (x_i - X)^2} \quad \{6\}$$

- where:
- x_i is the experimental value of ΔN for each case (i)
 - c_i is the predicted ΔN from equation {5} based on the experimental values of Δa , ΔK , PEN, and BSG for each case (i)
 - X is the experimental mean of all ΔN

It is generally accepted that the square of the correlation coefficient represents the percentage of the variance of the phenomenon (ΔN) being explained by the multiple regression analysis. Similarly, r^2 represents the percentage of variation of ΔN which is explained by the descriptive equation {5}. Using the data of $\Delta a/\Delta N$ collected experimentally,

the r^2 obtained was 0.60. This indicates that 60% of the behavior of a crack at the bone-cement interface can be explained in terms of the square of the stress intensity and the cube of the depth of cement penetration, moderated by a nonmonotonic influence from the bone strength.

The preceding analyses incorporated ΔK 's calculated as if no cohesive zone existed. Analysis was performed using Clech's results for a 4 mm cohesive zone at the interface. There was no significant difference between those results and the results reported.

Design and Evaluation of a Crack Arrestor

The observation that cracks tend to arrest temporarily, due to cement posts naturally occurring at the interface, suggested inserting additional posts in a regular, more controllable way. The number and size of posts which would optimally reduce crack propagation is available from equations {4} and {5}. For a constant cement post size, an increase in the number of posts will lead to a decrease in the area-fraction of bone present. A decrease in bone area-fraction gives rise to a decrease in bone strength. Thus in equation {5}, an artificial increase in $Post_N$ can lead to slight increases or decreases (dependent upon PEN and ΔK) in the crack propagation rate. Note from equation {4} however, that the same increase in $Post_N$ gives rise to a decrease in the crack propagation rate by increasing the total number of cycles. Therefore there must be an optimal artificial post density for an interface which is dependent upon an interface's existing bone strength, cement penetration, and stress state.

Equation {5} was therefore optimized as a function of the number of posts needed ($Post_N$) to maximize the number of load cycles which would produce a 20 mm crack length for several values of BSG and ΔK . The proposed posts were chosen to be 3 mm long and 3 mm diameter cylinders. Due to the many assumptions made at this point concerning bone strength, area fraction, and applying the previously reported results to three dimensions, specifics of the optimization procedure will not be reported and results obtained should be considered simply as being motivated by equation {5}.

The number of artificial posts ($Post_N$) desired at an interface ranged (as a function of bone density and ΔK) from 0 to 4 along the 20 mm interface. Thus, to implement the results for a 3 mm post size in the test specimen geometry, a 2 x 2 array of four posts 10 mm apart was chosen (Figure 6) in order to approximate average bone quality conditions.

The posts were bored (1 mm) centrally to facilitate insertion and promote cement interlock. Also, a center vent hole has been added to the device to alleviate lateral flow of cement upon device insertion. The metal device was grit blasted, passivated for 30 minutes in 30% V/V Nitric acid, and rinsed thoroughly in distilled water prior to specimen formation in accordance with ASTM standard F87. Using a steel template, four holes were drilled into the bone to a depth of 3

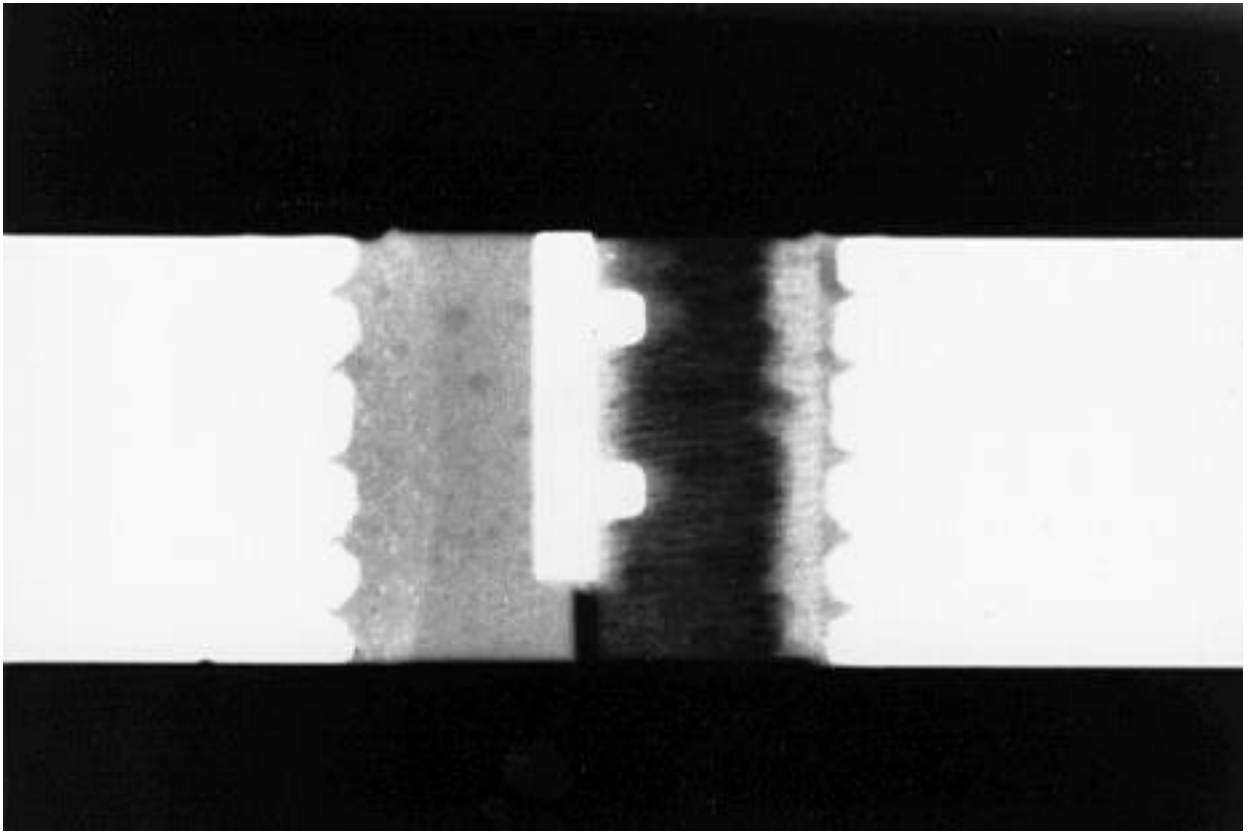


Figure 6: Radiograph of specimen A5D (with ‘crack arrestor’ device) in its four-point bent beam test configuration.

mm using a hand drill. This was done to accept the artificial posts of the device. The diameter of the holes was made slightly larger ($175\ \mu\text{m}$) than the 3 mm diameter of the posts. Fracture tests employing the same methodology previously described were performed.

Results of the Crack Arrestor Tests

Three initial fracture tests of the device were conducted. The raw data of these tests is reported in Table I. Of note in Table I is that none of the three specimens failed, but rather were stopped for separate reasons. Specimen A5d was simply halted after 500,000 cycles and statically loaded to failure (through a subinterface layer beneath the posts) at 706 Newtons. Specimen A6d (which was loaded at 311 N) behaved differently. At 20,200 cycles the cement-metal bond failed and the device pulled cleanly out of its cement mantle. It was then conjectured that the introduction of artificial metal posts may not be necessary, but rather the presence of large cement posts may be sufficient to arrest crack growth. Specimen A6d was refabricated with Simplex-P cement replacing the the metal posts by repolymerizing with the

existing cement mantle. Testing was halted at 83,000 due to failure through the bone stock. Specimen AZ5a was stopped after 216,000 cycles and not taken to failure but behaved similarly to A5d.

Crack extension vs cycles for specimens A5d and A6d is plotted in Figure 4. It can be seen from this figure that the addition of the artificial posts reduced crack mouth opening and the crack growth rate. More impressive is the fact that specimen A6d possessed a poorly penetrated interface within a high stress environment suggesting that inclusion of metal posts may compensate for poor cement penetration. The bone strength, penetration depth, and stress intensity data for these three specimens were then inserted into equation {5} to obtain perspective on the performance of the crack arrested cases in relation to the normal cases. All three crack arrested cases lasted longer than equation {5} predicted by a factor ranging from 2 to 30.

DISCUSSION

Increasing penetration dramatically increases the resistance to crack propagation rate (Figures 4 & 6). In fact it can be seen from equation {5} that the effect of cement penetration is greater (cubic) than that of the applied stress field (squared). This may indicate that with appropriate penetration, mechanical interface failure may be delayed.

The prediction equation {5} is based on limited material parameter value ranges as reported in Table I. Therefore an interface possessing material parameter values outside these ranges, specifically cement penetration depth, may not correspond to the reported results. There may be decreasing benefits of increasing cement penetration into bone over the appropriate penetration level mentioned previously, and in fact may exist an optimum penetration depth.

The effect of bone strength or bone density on the integrity of the interface is less apparent. This lack of clarity may be due in part to an 'optimum value' relation between bone strength and the tensile interface strength as described by Askew et al. [1]. Namely, as bone strength increases (allowing for a stronger interface), bone void size decreases accounting for less volume of penetrated cement. This points out that as there is an optimum penetration depth, there exists an optimum bone density for cement fixation.

Equations {5} and {1} are very similar, and in fact, equation {1} possesses almost the same relative variance as equation {5} (0.59 to 0.60). There could be several reasons why the hypothesized model is unable to explain crack growth at a higher level. There may exist independent variables other than those measured affecting crack behavior. Secondly, there may be some inherent error in the measurement of the independent variables. For instance, the cement penetration measured via radiography is based upon a two-dimensional image as opposed to the actual three-dimensional cement/bone interlock situation. Similarly, the measurement of the crack length was valid only along one side of the specimen which may be a false measure of the true crack tip. The bone area-fraction as opposed to the compressive

bone strength may be the optimal parameter to describe the interface. Overall, there seems to be some (as yet undefined) interaction between the cement penetration and the cancellous bone microstructure which would probably be of greater significance in the description of crack propagation at the interface.

The incorporation of Clech's cohesive zone model into the analysis provided no improvement in the description of crack growth. This could be due in part to the fact that Clech used a typical cohesive zone length which varied with the crack length from 1 to 5 mm. The inability in this study to use the actual cohesive zone length data for each individual specimen in the calculation of ΔK may have led to the insignificance of the cohesive zone model to the results. Clech also found that the cohesive zone played little beneficial role to the interface at short crack lengths and only really became effective at longer crack lengths.

Equation {5} does however account for 60% of the variance in the crack propagation rate. When representative interface conditions are chosen and applied to equation {5}, predicted results are reasonably close to the experimental results for trials with similar interface conditions (Figure 5). Perhaps most importantly, it can be seen in Figure 5 that both predicted and measured values of $\Delta a/\Delta N$ as a function of stress are markedly below (even under high penetration and high bone strength conditions) measurements made of isolated bone-cement [21].

Further demonstrating the interface's susceptibility to fatigue crack growth was the observation of a permanently deformed crack mouth opening. The permanent deformation of the interface noted in this study may facilitate the formation of fibrous tissue. Perhaps this deformation is due to plasticity of the cement, damage to the bone, slip of the cement spicules relative to bone, rupture of the cohesive zone, or a combination of all these factors.

The initial crack opening predicted by the finite element model (a rigid mesh of composite materials in pure bending) was virtually indistinguishable from the experimental results, implying that the initial interface between the bone and cement is very well connected. The fact that the opening begins to increase immediately with the application of cyclic load is an additional testimony to the interface's susceptibility to fatigue crack growth.

The designed posted device did, on a qualitative basis, dramatically reduce the crack propagation rate through the interface. It requires further testing to conclusively define its beneficial effects. The concept of crack arrestors could be implemented by direct placement of the artificial posts on a tibial component or by providing artificial cement posts of various sizes and depths in the bone matrix in accordance with the optimization of equation {5}, a surgically obtainable objective. Stress shielding of the bone surface between posts, formation of a subinterface failure zone, or varying tibial subchondral bone strengths are all factors which may effect the clinical implementation of the crack arrestor concept.

ACKNOWLEDGMENTS

This work was supported in part by grants MEA-8117106 and ECE-8501880 from the National Science Foundation.

REFERENCES

1. Askew MJ, Steege JW, Lewis JL, Ranieri R, Wixson RL: Effect of Cement Pressure and Bone Strength on Polymethylmethacrylate Fixation. *J Ortho Res* 1:412-420, 1984
2. Beaumont PW, Young RJ: Failure of Brittle Polymers by Slow Crack Growth. *J Mat Sci* 10:1334-1342, 1975
3. Behri JC, Bonfield W: Fracture Mechanics of Bone – The Effect of Density, Specimen Thickness, and Crack Velocity on Longitudinal Fracture. *J Biomechanics* 17:25-34, 1984
4. Carter DR, Hayes WC: The Compressive Behavior of Bone as a Two-Phase Porous Structure. *J Bone Joint Surg* 59-A:954-962, 1977
5. Charnley J: *Acrylic Cement in Orthopaedic Surgery*. Baltimore MD, Williams and Wilkins, 1970
6. Clech JP, Keer LM, Lewis JL: A Finite Element Technique for Determining Mode I Stress Intensity Factors: Application to No-Slip Bimaterial Crack Problems. *Computers & Structures* 24, 1986
7. Clech JP, Keer LM, Lewis JL: A Model of Tension and Compression Cracks With Cohesive Zone at a Bone-Cement Interface. *J Biomech Eng* 107:175-182, 1985
8. Davies JP, Harris WH: Severe Weakness of Bone-Cement Retrieved After in vivo Service in Man. *Trans 35th ORS* 14:393, 1989
9. Freeman MAR, Bradley GW, Revell PA: Observations Upon the Interface Between Bone and Polymethylmethacrylate Cement. *J Bone Joint Surg* 64-B:489-493, 1982
10. Freitag TA, Cannon SL: Fracture Characteristics of Acrylic Bone Cements: I. Fracture Toughness. *J Biomed Mat Res* 10:805-828, 1976
11. Gates EI, Carter DR, Harris WH: Comparative Fatigue Behavior of Different Bone Cements. *Clinical Orthopaedics* 189:294-299, 1984
12. Kolbel R, Bergmann G, Boenick U: Mechanical Properties of the Cement/Bone Bond. In: *Engineering in Medicine* 2, ed by Schaldach and Hehmen, New York, Springer-Verlog, 1976, pp 347-357
13. Krause WR, Krug W, Miller J: Strength of the Cement-Bone Interface. *Clinical Orthopaedics* 163:290-299, 1982
14. Lewis JL, Askew MJ, Jaycox DP: A Comparative Evaluation of Tibial Component Designs of Total Knee Prostheses. *J Bone Joint Surg* 64-A:129-135 1982

15. Lewis JL, Nicola T, Keer LM, Clech JP, Steege JW, Wixson RL: Failure Processes at the Cancellous Bone-PMMA Interface. *Trans 31st ORS* 10:144, 1985
16. Mak AF, Lewis JL: Fracture Mechanics of the PMMA/Cancellous Bone Interface. *1980 ASME Advances in Bioengineering* pp 209-212, 1980
17. Nicola TL: Failure of the Cancellous Bone-Cement Interface in Total Knee Joint Replacements. M.S. dissertation, Northwestern University, Evanston IL, 1984
18. O'Conner DO, Burke DW, Davies JP, Harris WH: S-N Curve for Centrifuged and Uncentrifuged PMMA. *Trans 31st ORS* 10:325, 1985
19. Radin EL, Rubin CT, Thrasher EL, Lanyon LE, Crugnola AM, Schiller AS, Paul IL, Rose RM: Changes in the Bone Cement Interface After Total Hip Replacement. *J Bone Joint Surg* 64-A:1188-1200, 1982
20. Reckling FW, Asher MA, Dillow WL: A Longitudinal Study of the Radiolucent Line at the Bone-Cement Interface Following Total Joint Replacement Procedures. *J Bone Joint Surg* 59-A:355-358, 1977
21. Rimnac CM, Wright TM, McGill DL: The Effect of Centrifugation on the Fracture Properties of Acrylic Bone Cement. *J Bone Joint Surg* 68-A:281-287, 1986
22. Robinson RP, Wright TM, Burstein AH: Mechanical Properties of Polymethylmethacrylate Bone Cements. *J Biomed Mat Res* 15:203-208, 1981
23. Sih GC, Berman AT: Fracture Toughness Concept Applied to Methylmethacrylate. *J Biomed Mat Res* 14:311-324, 1980
24. Stark CF: Fracture and Fatigue Characteristics of Bone Cements. *J Biomed Mat Res* 13:339-342, 1979
25. Tibrewal SB, Grant KA, Goodfellow JW: The Radiolucent Line Beneath the Tibial Components of the Oxford Meniscal Knee. *J Bone Joint Surg* 66-B:523-529, 1984
26. Walker PS, Soudry M, Ewald FC, McVickar H: Control of Cement Penetration in Total Knee Arthroplasty. *Clinical Orthopaedics* 185:155-164, 1984
27. Wright TM, Hayes WC: Fracture Mechanics Parameters for Compact Bone - Effects of Density and Specimen Thickness. *J Biomechanics* 10:419-430, 1977

TABLE I: Data

Test Number	Bone Type	Bone Strength		Cement Penetration Depth		Cement Application Pressure [KPa]	Applied Bending Load [N]	Initial Crack length opening		Failure Cycles [log(N)]
		[MPa]	Grade	[mm]	Grade			[mm]	[μm]	
N1a1	tibia	5.34	2	0.10	1	197	178	-	-	-
N1a2	tibia	5.34	2	4.08	3	197	489	4.9	-	2.50
N3b	tibia	4.82	2	1.32	1	049	222	-	-	-
N3d	tibia	4.62	2	3.13	2	122	267	5.2	-	2.84
N4a	femur	5.21	2	3.67	2	197	489	5.5	-	3.42
N4b	femur	2.49	1	1.70	1	036	133	-	-	-
N5b	femur	5.69	2	1.75	1	121	356	-	-	-
N5c	femur	2.24	1	2.77	1	121	133	-	-	-
N5d	femur	4.75	2	4.61	3	197	267	-	-	-
N6b	femur	2.10	1	2.78	1	076	178	-	-	-
S1a	femur	5.06	2	2.29	1	138	178	4.5	50	5.44
S1b	femur	8.47	3	2.48	1	138	178	5.3	72	4.16
S1c	femur	3.58	2	3.89	2	138	178	5.0	48	5.71
S3b	femur	8.38	3	3.57	2	138	178	4.4	36	≥ 5.74
S6a	femur	3.79	2	4.57	3	138	178	5.0	-	≥ 5.49
S6b	femur	7.76	3	5.30	3	138	356	5.4	120	3.30
S6c	femur	3.79	2	5.94	3	138	178	4.3	-	≥ 5.20
S10a	femur	5.25	2	3.54	2	138	178	5.2	37	5.73
S10c	femur	8.09	3	4.56	3	138	267	4.9	61	5.35
S13a1	femur	9.64	3	0.10	1	-	178	-	-	0.00
S13a2	femur	9.64	3	3.50	2	-	311	4.1	45	5.75
S13b	femur	3.77	2	6.93	3	138	178	5.2	52	5.58
Z3a	tibia	5.04	2	1.45	1	035	035	4.0	50	4.92
Z5a	tibia	3.00	2	1.40	1	035	067	4.5	42	4.17
Z9a	tibia	1.15	1	1.12	1	035	089	4.4	107	3.00
Z11a	tibia	1.97	1	0.51	1	035	051	4.8	52	1.48
mean		4.81		2.96		116	192	4.8	59	≥ 5.27
standard dev.		2.33		1.77		60	127	0.5	26	5.33
A5d*	femur	3.99	2	3.73	2	-	178	5.2	32	≥ 5.70
A6d•	femur	8.42	3	2.80	1	-	311	5.0	42	≥ 4.92
AZ5a*	tibia	3.00	2	5.60	2	-	267	4.4	32	≥ 5.33
• bone fracture										
* test stopped										
mean*		5.14		4.04			252	4.9	35	≥ 5.43
standard dev.*		2.89		1.43			68	0.4	6	5.33

* Crack arrestor trials